npj computational materials

www.nature.com/npjcompumats

ARTICLE OPEN

Check for updates

Electron-phonon coupling and spin fluctuations in the Ising superconductor $NbSe_2$

S. Das[1,2]✉, H. Paudyal[3], E. R. Margine[3], D. F. Agterberg[4] and I. I. Mazin[1,2]

Ising superconductivity, observed in $NbSe_2$ and similar materials, has generated tremendous interest. Recently, attention was called to the possible role that spin fluctuations (SF) play in this phenomenon, in addition to the dominant electron–phonon coupling (EPC); the possibility of a predominantly triplet state was discussed and led to a conjecture of viable singlet–triplet Leggett oscillations. However, these hypotheses have not been put to a quantitative test. In this paper, we report first principle calculations of the EPC and also estimate coupling with SF, including full momentum dependence. We find that: (1) EPC is strongly anisotropic, largely coming from the $K - K'$ scattering, and therefore excludes triplet symmetry even as an excited state; (2) superconductivity is substantially weakened by SF, but anisotropy remains as above; and, (3) we do find the possibility of a Leggett mode, not in a singlet–triplet but in an $s_{++} - s_{\pm}$ channel.

npj Computational Materials (2023)9:66 ; https://doi.org/10.1038/s41524-023-01017-4

INTRODUCTION

Revolutionary progress in the growth and exfoliation of single atomic layers over the last two decades has led to a new era of scientific discoveries and technological innovation. Following graphene, transition metal dichalcogenides (TMDs) have taken the spotlight, as a treasure trove for a plethora of novel quantum phenomena. One of the significant discoveries in recent years was the phenomenon of the so-called Ising superconductivity, driven by spin–orbit (SO) coupling combined with the absence of the inversion symmetry[1–10]. Proximity effects and interfaces of Ising superconductors with other layered materials such as topological materials[11,12] and monolayer TMDs, such as doped TaS_2 and $TaSe_2$[8,13], or with two-dimensional (2D) magnetic layered materials, such as CrI_3[14,15] and VI_3[16], could lead to interesting device applications for quantum information storage and spintronics.

The lack of inversion symmetry and SO coupling in monolayers of 2H-$NbSe_2$ leads to splitting of the electronic bands near the K point, and its corresponding inversion counterpart, $K' = -K$, in the Brillouin zone (BZ). The magnitude of this splitting due to spin–orbit effects is considerably larger than the superconducting order parameter[13,17]. Because of this splitting, the formally s-wave singlet superconducting state well known in the bulk $NbSe_2$, splits into two mixed states: singlet (S) and triplet (T) states combine to form an S + T state on one SO partner and an S – T state on the other. The same is true about the inversion-related partners, e.g., the outer Fermi contours around K and K'[17]. The emerging phenomenon was duly dubbed "Ising superconductivity" (IS). While in most experimental probes the two IS partners combine to form a (nearly) pure S state, the incipient triplet component manifests itself in many notable ways, most famously in the formally infinite thermodynamic critical field along the *ab* layer plane.

Recent first-principles calculations, combined with some limited experimental data, strongly suggest that bulk $NbSe_2$ is close to a magnetic instability, and the undistorted monolayers are even closer[17–19] (and also likely for similar TMD superconductors). This fact led to speculations that triplet pairing, even if not a leading instability, may play an important role in Ising superconductivity in $NbSe_2$[17]. Recent observation of a low-temperature tunneling mode in $NbSe_2$ monolayers was tentatively interpreted as a singlet–triplet Leggett mode[20].

Recently, we investigated the full momentum-dependent spin susceptibility[21] in $NbSe_2$ monolayers[19], and found that it is rather strongly peaked at a particular wave vector, close to $\mathbf{q} = (0.2, 0)$ in the 2D Brillouin zone. At the same time, experimental and density functional theory (DFT) calculations of charge density waves[22–26] and superconductivity[4,10,20,26,27] for some bulk[17,22,28,29] and 2D TMDs[17,30–34] have been reported. A subsequent first-principles study claimed[17] that density functional calculations overestimate the superconducting transition temperature in monolayer $NbSe_2$. Together with the indications of strong spin fluctuations (SF) in this class of materials, it strongly suggests that a proper quantitative analysis of the pairing state in $NbSe_2$, and likely in other Ising superconductors, is not possible without the simultaneous accounting of the anisotropic electron–phonon coupling (EPC) and SF-induced interaction.

In this paper, we present such an analysis and find several expected and some rather unexpected results. First, in agreement with existing calculations of bulk and 2D TMDs, the standard DFT calculations of EPC strongly overestimate the transition temperature in monolayer $NbSe_2$ (far beyond typical inaccuracies of the method). Second, including on the same footing SF-induced interaction (using the previously calculated SF spectrum[19]) brings the calculations in agreement with the experiment (including a proper frequency cutoff for SF is essential). Third, the calculated EPC is exceptionally anisotropic, with the lion's share of the coupling coming from the same-spin $K - K'$ scattering. The calculated gap distribution, formally speaking, should be visible in tunneling experiments, and it has not been observed so far. We discuss possible reasons for why the small gap on the Γ Fermi surface pocket has so far eluded detection.

[1]Department of Physics and Astronomy, George Mason University, Fairfax, VA 22030, USA. [2]Quantum Science and Engineering Center, George Mason University, Fairfax, VA 22030, USA. [3]Department of Physics, Applied Physics, and Astronomy, Binghamton University-SUNY, Binghamton, NY 13902, USA. [4]Department of Physics, University of Wisconsin, Milwaukee, WI 53201, USA. ✉email: sdas28@gmu.edu

Background landscape

Tunneling. Tunneling experiments are an indispensable tool for the discernment of the quantitative as well as qualitative nature of superconducting order parameter in unconventional superconductivity[4]. In ref. [20], it is pointed out that the different character of the dominant Nb orbitals on the Γ and *K* Fermi surface pockets suggest that their tunneling probability through vacuum or insulating barrier should be different. The fact that the calculated superconducting gap is rather different at the two sets of pockets suggest that this issue deserves a closer look.

One possible explanation for the lack of observation of a smaller gap is that, due to impurity scattering, the gap averages to one uniform value. We do not find this likely. Indeed, the observed $2\Delta/T_c$ ratio is noticeably larger than the weak-coupling value of 3.54, and our calculations are far from the strong coupling regime where such an enhancement would be possible. Rather, our larger (*K*) gap agrees consistently with the experiment. This calls into question, why the second, smaller gap is not seen in the experiment? We do not have an answer yet, but we can add to the body of known facts, our calculations of the partial character of Se p_z at the Fermi level. Indeed, in STM experiments, it is rather clear that the main signal comes from Se atoms, and this orbital is the most extended along the out-of-plane direction, so it is expected to dominate the STM spectra. We show this character as the faux map in Fig. 2.

Interestingly, while on average the Γ pocket has a larger content of this character, there are hot spots along the $K-M$ direction that are expected to have the largest tunneling probability; taking the calculated value of the superconducting gap at this point yields a rather good agreement with the experiment. On the other hand, while the difference between the tunneling current from p_z orbitals is exponentially higher than that from the $p_{x,y}$ ones, the dependence on the p_z weight is just linear, so, in principle, one would expect to see subgap features corresponding, first of all, to the Γ pocket gap approximately twice smaller than the maximal gap.

In order to address the nature of the superconducting gap, scanning tunneling measurements were performed and reported on few-layer $NbSe_2$[31]. The superconducting gap as well as the critical temperature (T_c) have been found to decrease with increasing the number of layers. In particular, the gap values measured at 0.3 K exhibited a reduction by more than a factor of 2 from 1.3 meV in the bulk to 0.6 meV in the bilayer. Unfortunately, no tunneling current was detectable in the monolayer devices, most likely due to the difficulty of obtaining a clean $NbSe_2$–hBN interface. The decrease in the T_c has been found to be well described by a linear dependence with the inverse thickness, with the temperature dropping from 7.0 K in bulk to 4.7–4.8 K and 2.0–2.5 K in bilayer and monolayer, respectively. This drastic decrease in both the measured superconducting gap and critical temperature has been assigned to the surface energy contribution imposed by the boundary condition upon the electronic wave function. Further, it has been conjectured that while for up to five layers or higher, the gap is considerably anisotropic, the anisotropy disappears and the gap obeys the isotropic Bardeen–Cooper–Schrieffer (BCS) gap equations for the bilayer[31]. The hypothesis that the incommensurate charge density wave is enhanced by the simultaneous existence of superconductivity in monolayer $NbSe_2$ has also been proposed[27].

Experimental results vs magnetic and electron–phonon coupling calculations. Superconductivity in bulk $NbSe_2$ has been studied extensively both experimentally and theoretically, and the superconducting transition temperature T_c has been experimentally identified as ~7 K[35]. Compared to bulk, T_c of monolayer $NbSe_2$ is about half, up to ~3.5 K in best samples (it is often as low as 1 K)[3,8]. It was argued that the above is due to the pair-breaking effect of magnetic moments associated with Se vacancies[7].

State-of-the-art first-principles calculations that usually deliver accurate outcomes for superconductors where the pairing is entirely due to EPC, overestimate the T_c in bulk $NbSe_2$[22] and isostructural NbS_2[26]. In the latter case, calculations using Eliashberg theory yield a T_c and a zero-temperature gap a factor of ~3 and 4 larger than experiment, respectively[26]. At the same time, the experimentally measured spin susceptibility, χ_s, in bulk $NbSe_2$ was reported to be $\chi_s \sim 3\times10^{-4}$ emu mole^{-1}[36], which significantly exceeds the bare bulk Pauli susceptibility $\chi_0 \sim 0.87\times10^{-4}$ emu mole^{-1}. DFT calculations render $\chi_s = 4.2\times10^{-4}$ emu mole^{-1} (see refs. [17,19]), 40% larger that in the experiment—a common overestimation in itinerant systems, indicating that SF are strong in the system.

Recently, we have calculated the static **q**-dependent DFT susceptibility in $NbSe_2$ monolayer[19], and rescaled it to account for the fluctuational reduction; the latter was deduced from the known experimental data for the bulk compound. Together with the standard formalism for calculating EPC, this forms the basis for addressing superconductivity in monolayer $NbSe_2$ from first principles.

Role of charge density waves. The role played by charge density waves in either assisting or opposing superconductivity has been a matter of active debate in the field of unconventional superconductivity. Several recent papers[32,33] ascribe the notorious overestimation of the superconducting temperature and order parameter to the charge density wave (CDW) effects. We do not believe that CDW alone provides a comprehensive explanation, if at all, for the following reasons:

- First of all, overestimation takes place both in the bulk and in single layer calculations of $NbSe_2$[22,29,33]. Yet in $NbSe_2$ suppression of the CDW by pressure or disorder has only a minor effect on the T_c[22,37–39].
- NbS_2 does not exhibit a CDW phase, yet the problem of overestimation there is as severe, if not more so[26].
- It was shown that in bulk $NbSe_2$ anharmonicity strongly suppresses the tendency to form the CDW[22], hence it is likely that standard DFT calculations overestimate the CDW amplitude and leads to the partial gapping of the Fermi surface. Bulk calculations for $NbSe_2$, accounting for anharmonicity to suppress CDW at elevated pressure, extrapolate to $T_c \approx 12.3$ K and $\lambda \approx 1.4$ at zero pressure, a considerable overestimate[22].
- Overestimation of the T_c was also recently attributed to the empirical treatment of the Coulomb interaction in the Eliashberg formalism compared to the superconducting density functional theory[29]. Assuming a value of the Coulomb pseudopotential $\mu^* = 0.11$ yielded a superconducting $T_c = 16$ K, whereas a significantly higher value of $\mu^* = 0.28$ was necessary to replicate the experimental outcome. Note that, while resorting to an unusually high value of μ^* reproduces the experimental gap, such Coulomb interactions are not physical even for low-density metals, since the value of μ^* (as opposed to μ) is set by $\log(E_F/\omega_{ph})$, and not by the bare Coulomb coupling.
- The resistivity in the normal state shows absolutely no detectable feature at the CDW temperature[23]. If, as suggested in ref. [33], CDW reduces the EPC constant by a factor of seven, the effect on normal transport would have been dramatic.
- In recent experiments[20], suppressing CDW in single layer $NbSe_2$ by disorder (such as Mo doping) led to T_c simultaneously suppressed.

For these reasons, we believe that the effect of CDW on superconductivity in previous works was overestimated and CDW plays at best a small role[38,39] in suppressing superconductivity. Instead, in this paper we put emphasis on the pair-breaking effect of magnetic interactions. Experimental results indicate that while

Table 1. A summary of the experimental results of key parameters pertaining to superconductivity in bulk and monolayer $NbSe_2$ with CDW, and with CDW removed by pressure (p) or disorder (d).

	Bulk, CDW	Bulk, no CDW (p)	Bulk, no CDW (d)	Monolayer, CDW
T_c (K)	7.2[37–39]	8.3[38], 8.4[39]	7.0[37]	3.5[3,10]
$\frac{dH_{c2}}{dT}\|_{T\to T_c}$ (T/K)	0.55[38], 0.9 [39]	0.42 [38], 0.36[39]	-	0.62[1,3]

Not enough data exist to assess the trends in the superconducting gap, or in $H_{c2}(0)$, but $dH_{c2}/dT|_{T\to T_c}$ for the out-of-plane fields can be compared. Experimental results indicate that the CDW affects the pairing strength rather little. Note that the cited references ascribe the changes in the H_{c2} to the changes in the Fermi velocity, not in the order parameter.

T_c increases linearly with systematic increase in pressure in the CDW phase, the slope of H_{c2} changes non-monotonically and hence does not affect the gap size/ pairing size (Table 1). The authors further conclude that the changes in the gap size are related rather to that of the Fermi velocity, which is consistent with the fact that the CDW does not change the pairing strength too much.

RESULTS

Theoretical basis

The recipe for calculating electron–phonon interactions from first principles is well established[40,41]. However, the incorporation of the effects of spin fluctuation warrants reevaluation of the hitherto established protocol. A formalism incorporating spin-fluctuation effects alongside electron–phonon coupling would set the stage to delineate the concomitant landscapes of conventional and unconventional superconductivity. The momentum-dependent Eliashberg spectral function is given by:

$$\alpha^2F_{\rm ep}(\mathbf{k},\mathbf{k}',\omega) = N_{\rm F}\sum_{\nu}|g^{\nu}_{\mathbf{k},\mathbf{k}'}|^2\delta(\omega-\omega_{\mathbf{q}\nu}), \tag{1}$$

where $N_{\rm F}$ is the density of states per spin at the Fermi level, $\mathbf{k}$ denotes the combined electron band and momentum index, $g^{\nu}_{\mathbf{k},\mathbf{k}'}$ are the screened electron–phonon matrix elements, and $\omega_{\mathbf{q}\nu}$ are the phonon frequencies for a phonon with wavevector $\mathbf{q} = \mathbf{k} - \mathbf{k}'$ and branch index ν.

A systematic incorporation of spin fluctuations is less well established, even though the problem goes back to the 1960s[42]. The simplest recipe is summarized in ref. [43], and stipulates that the effective pairing interaction in the singlet channel is given by the Eliashberg function $\alpha^2F_{\rm sf}(\mathbf{k},\mathbf{k}',\omega)$, defined through the dynamical spin susceptibility $\chi_{\mathbf{k}-\mathbf{k}'}(\omega)$ and (in the modern DFT parlance) the Stoner factor I:

$$\alpha^2F_{\rm sf}(\mathbf{k},\mathbf{k}',\omega) = -\frac{3}{2\pi}N_{\rm F}I^2{\rm Im}[\chi_{\mathbf{k}-\mathbf{k}'}(\omega)]. \tag{2}$$

In the triplet channel, the sign is positive (attraction) and the spin-rotation factor 3 is replaced by 1. In practice, the static integrated version of Eq. (2), calculated as the Fermi surface average, is universally used:

$$\lambda_{\rm sf} = -\frac{3}{2}N_{\rm F}\langle I^2{\rm Re}\chi_{\mathbf{q}}\rangle_{\mathbf{q}}. \tag{3}$$

More elaborate versions, taking into account ladder diagrams in addition to polarization bubbles, have also been put forward in the following years, most notably by Fay and Appel[44], but in proximity to a magnetic instability the only resonant term is the one given by Scalapino[43,45]. The non-resonant part is usually assumed to be incorporated in the Coulomb pseudopotential.

Equation (3) has one serious problem however: it completely neglects retardation effects, implicitly assuming that the characteristic time scale for the spin fluctuations is the same as for phonons, which is rarely the case. Because of this, practical applications of this formalism are plagued by overestimating the SF effect compared to that of the EPC. For instance, Bekaert et al.[46] recently reported calculations for FeB_4, and found that Eq. (3) severely overestimates the effect of SF. To compensate, they have scaled the result by the partial density of the Fe-character states at the Fermi level, even though the original formalism does not provide for that and hybridization effects are supposed to be included in the Stoner factor I.

In fact, when a proper frequency dependence is included, the difference in the energy scales between phonons and SF logarithmically reduces the SF-induced interaction, pretty much the same way as the Coulomb repulsion is being renormalized to μ^*[47,48].

Over the years, several recipes have been implemented which follow assumptions similar to the above[49–51], albeit slight modifications for incorporating spin fluctuations following Scalapino's formalism. The prevalence of the analytical fitting of model parameters primarily rests upon the fact that: (i) A detailed experimental measurement of the frequency dependence of spin susceptibility in monolayer $NbSe_2$ has been lacking in the literature, rendering a systematic comparison difficult, and (ii) The primary criterion underlying our fitting is that as long as the superconducting T_c is fit reasonably well, the structure of the superconducting gap does not change by comparing various popular forms of the model parameter[49–51]. Based on the above, we provide a recipe for modeling the parameters, $\omega_{\rm sf}$ and a in order to evaluate the BCS superconducting gap. We include this renormalization implicitly by using Eq. (2) instead of Eq. (3), such that[49,50]

$$\chi_{\mathbf{k}-\mathbf{k}'}(\omega) = \chi_{\mathbf{k}-\mathbf{k}'}(0)P(\omega), \tag{4}$$

where

$$P(\omega) = \frac{a\omega}{(\omega-\omega_{\rm sf})^2+a^2}\theta(\omega_{\rm c}-\omega), \tag{5}$$

with $\omega_{\rm c} = 1$ eV the Matsubara frequency cutoff, $\omega_{\rm sf} = 0.5$ eV a characteristic frequency for spin fluctuations, and $a = 0.1$ a scaling parameter. We estimate the latter two from the calculation of the noninteracting, constant matrix element (Lindhard) susceptibility[21] using the DFT band structure (Fig. 1a), and then further adjust it slightly to match the experimental T_c.

The full formalism now appears as follows:

$$Z_{\mathbf{k}}(\omega_j) = 1 + \frac{\pi T}{N_{\rm F}\omega_j}\sum_{\mathbf{k}'j'}\frac{\omega_{j'}\delta(\epsilon_{\mathbf{k}'}-\epsilon_F)}{\sqrt{\omega_{j'}^2+\Delta^2_{\mathbf{k}'}(\omega_{j'})}} \times\left[\lambda^{\rm ep}_{\mathbf{k},\mathbf{k}'}(\omega_{j-j'}) - \lambda^{\rm sf}_{\mathbf{k},\mathbf{k}'}(\omega_{j-j'})\right] \tag{6}$$

$$Z_{\mathbf{k}}(i\omega_j)\Delta_{\mathbf{k}}(i\omega_j) = \frac{\pi T}{N_{\rm F}}\sum_{\mathbf{k}'j'}\frac{\Delta_{\mathbf{k}'}(\omega_{j'})\delta(\epsilon_{\mathbf{k}'}-\epsilon_F)}{\sqrt{\omega_{j'}^2+\Delta^2_{\mathbf{k}'}(i\omega_{j'})}} \times\left[\lambda^{\rm ep}_{\mathbf{k},\mathbf{k}'}(\omega_{j-j'}) + \lambda^{\rm sf}_{\mathbf{k},\mathbf{k}'}(\omega_{j-j'}) - \mu^*_{\rm c}\right], \tag{7}$$

This set of coupled nonlinear equations relates the momentum-dependent quasi-particle mass renormalization function $Z_{\mathbf{k}}(\omega_j)$ and superconducting gap function $\Delta_{\mathbf{k}}(\omega_j)$. Here, $\epsilon_{\mathbf{k}}$ are the Kohn–Sham eigenvalues, $i\omega_j = i(2j+1)\pi T$ (j integer) are the fermionic Matsubara frequencies at temperature T, and $\lambda^{\rm ep}_{\mathbf{k},\mathbf{k}'}(\omega_j)$ and $\lambda^{\rm sf}_{\mathbf{k},\mathbf{k}'}(\omega_j)$ describe the coupling of electrons to phonons and spin fluctuations. The two coupling terms can be expressed based

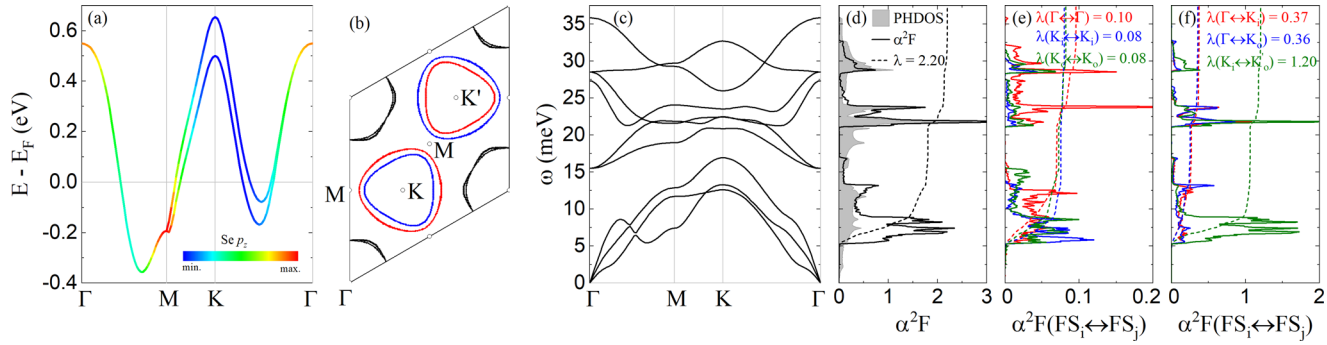

Fig. 1 Electron–phonon interaction and intra/inter-pocket Eliashberg spectral function. a Calculated band structure with SO coupling in monolayer $NbSe_2$. The color along each band denotes the relative Se p_z character according to the color bar. The orbital character is taken from a calculation without SO coupling. **b** Cross section of the Fermi surface with SO coupling in monolayer $NbSe_2$. Red and blue dots at the K and K' contours denote spin-up and spin-down states. Here "o" and "i" stand for the outer and inner pocket around the corresponding point. Calculated (**c**) phonon dispersion, **d** phonon density of states, isotropic Eliashberg spectral function $\alpha^2F(\omega)$ and integrated EPC $\lambda(\omega)$. Decomposition of $\alpha^2F(\omega)$ and $\lambda(\omega)$ corresponding to (**e**) intra-pocket $\Gamma-\Gamma$ (red), K_i-K_i plus $K'_i-K'_i$ (blue), and K_o-K_o plus $K'_o-K'_o$ (green) scattering, and (**f**) inter-pocket $\Gamma-K_i$ plus $\Gamma-K'_i$ (red), $\Gamma-K_o$ plus $\Gamma-K'_o$ (blue), and $K_i-K'_o$ plus $K_o-K'_i$ (green) scattering.

on their respective Eliashberg spectral functions:

$$\lambda^{\mathrm{ep}}_{\mathbf{k},\mathbf{k}'}(\omega_{j-j'}) = \int_0^\infty d\omega \frac{2\omega\alpha^2F_{\mathrm{ep}}(\mathbf{k},\mathbf{k}',\omega)}{(\omega_j-\omega_{j'})^2+\omega^2}, \tag{8}$$

$$\lambda^{\mathrm{sf}}_{\mathbf{k},\mathbf{k}'}(\omega_{j-j'}) = \int_0^\infty d\omega \frac{2\omega\alpha^2F_{\mathrm{sf}}(\mathbf{k},\mathbf{k}',\omega)}{(\omega_j-\omega_{j'})^2+\omega^2}. \tag{9}$$

A closer look at the expressions (6) and (7), reveals the fact that the presence of spin fluctuations enhances the quasi-particle mass renormalization by increasing the effective mass of the carriers and suppresses superconductivity in the singlet channel by reducing the effective coupling strength. The credence that this formalism will provide a more fitting description of the experimental superconducting order parameter by establishing electron–phonon coupling and spin fluctuations on an equal footing remains to be ascertained.

Computational results

Figure 1a, b shows the calculated electronic structure of monolayer $NbSe_2$. The Fermi surface consists of three distinct sheets, one centered around the Γ point and two around K and K'. The broken inversion symmetry in the monolayer leads to the SO interaction splitting each pocket into a pair with spin-up and spin-down states. At the K and K' contours, the states with spin-up and spin-down characters are depicted as red and blue dots in Fig. 1b. Since the splitting near Γ is minor, we do not distinguish the states with different spins around this point.

As it has already been pointed out in previous studies[32,33,52], the lowest-energy branch of the phonon spectra is strongly anharmonic, displaying negative frequencies along the Γ M and MK directions. To take care of this unstable mode that drives the system into a CDW transition, we used a larger electronic smearing. With the exception of the soft acoustic mode that hardens and becomes positive, there is no other significant change in the phonon dispersion when the electronic broadening is increased from 0.01 to 0.03 Ry. Our choice of a 0.025 Ry smearing results in a phonon spectrum (see Fig. 1c) which is in good agreement with full anharmonic calculations[52].

Based on the topology of the Fermi surface, the Eliashberg spectral function and the EPC strength can be decomposed into intra- and inter-pocket scattering contributions. As shown in Fig. 1e, f, the inter-pocket scattering is dominant, with more than 50% of the coupling coming from the inter-pocket scattering between the K and K' pockets of the same-spin character (i.e., between the states on the inner and outer contours at K and K' and vice versa). In agreement with previous calculations[33], the superconducting gap is found to be strongly anisotropic and, in the first approximation, can be described as consisting of two gaps (Fig. 2a). The smaller gap is associated with the Γ Fermi sheets, while the larger gap belongs to the K and K' sheets. Using $\mu^*_c = 0.15$, our calculations yield a superconducting critical temperature of 19 K, overestimating even the largest reported experimental value of ~3.5 K [3,10]. As discussed, we attribute this discrepancy mainly to the pair-breaking effect of spin fluctuations, and not due to the CDW.

We solve again the anisotropic Eliashberg equations now accounting for spin fluctuations along with the electron–phonon coupling. The superconducting gap on the Fermi surface at low temperature and the gap distribution as a function of temperature

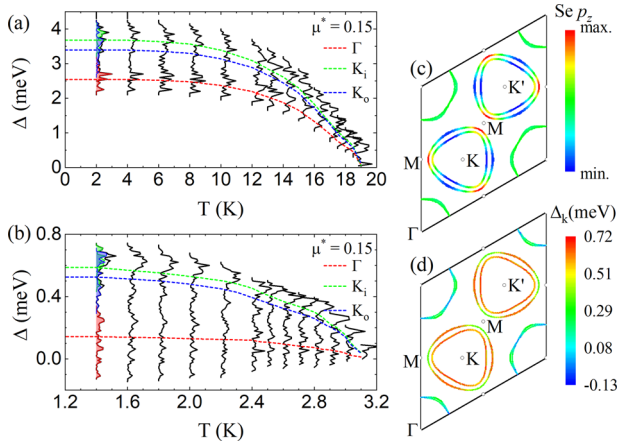

Fig. 2 Superconducting gap without and with spin-fluctuation interaction. Energy distribution of the superconducting gap as a function of temperature computed over the full BZ by solving the anisotropic Eliashberg Eqs. (6) and (7) (**a**) without and (**b**) with the inclusion of spin fluctuations. Each curve represents a histogram of gap values at a particular T shown on the x axis; the height of the histograms is related to the number of states on the FS with that superconducting gap energy. The colored shaded areas at lowest temperature indicate data belonging to different FS sheets: Γ (red), K_i (green), and K_o (blue). The dashed red, green, and blue curves are averages of the anisotropic solutions. **c** Cross section of the Fermi surface with Se p_z character. **d** Momentum-resolved superconducting gap $\Delta_{\mathbf{k}}$ on the Fermi surface corresponding to the anisotropic Eliashberg calculations with the inclusion of spin fluctuations at $T = 1.4$ K.

calculated in the presence of SF are displayed in Fig. 2b, d. Under the influence of spin fluctuations, the two-gap structure is maintained, but the superconducting gap and the corresponding critical temperature are drastically reduced. Using a spin-fluctuation frequency $\omega_{sf} = 0.5$ eV, $a = 0.1$, and $\mu_c^* = 0.15$, we get $T_c = 3.2$ K in good agreement with the experimental values.

DISCUSSION

Let us first start with the results of the EPC calculation only, as these already uncover unexpected and important physics. The first observation, as mentioned, is that unmitigated EPC is way too strong to be consistent with the experiment, calling for spin fluctuations. Regardless of this, the calculated EPC is strongly nonuniform. The EPC is strongly dominated by the $K_i - K'_o$ and the equal by symmetry $K_o - K'_i$ coupling (note that $\lambda_{ij} = V_{ij}N_j$, where V is a symmetrical matrix and N_j is partial DOS). This implies that the order parameter will be similar in magnitude on the K sheets. The order parameter on the Γ pockets will be mostly induced by the interband proximity effect and is expected to be relatively small. All this is corroborated by our full Eliashberg calculations.

Before analyzing the pairing symmetry, we shall make an important note. In regular, non-Ising superconductors (i.e., with inversion symmetry and not spin–orbit split, but possibly SO-influenced) a standard way to analyze the pairing symmetry, whether on the level of the simple linearized BCS equations, or full anisotropic Eliashberg calculations, is to assign a complex value of the order parameter to each point on each Fermi surface, and proceed from there. The standard signature of a triplet pairing is the phase shift of π (i.e., a sign changed between the **k** and −k points).

Importantly, this is not a unique procedure and depends upon the choice of the phase gauge in the normal state between different **k**-points, which sometimes leads to nontrivial ramifications[53]. It becomes even more nontrivial in case of an Ising superconductor. To illustrate this, we will use as order parameters anomalous averages as defined in ref. [17]:

$$\begin{aligned} d_{o,\mathbf{k}} &= \overline{|K,o,\uparrow\rangle|K',o,\downarrow\rangle} \\ d_{i,\mathbf{k}} &= -\overline{|K,i,\downarrow\rangle|K',i,\uparrow\rangle} \end{aligned} \tag{10}$$

Here, $d_{o,\mathbf{k}}$ corresponds to a Cooper pair with one electron on the outer shell of a K pocket with the spin-up, and the other on the outer shell of the opposite K' pocket, with the spin down, and similarly for $d_{i,\mathbf{k}}$. At this point, it is instructive to compare this with another material that has a nearly identical Fermi surface, also with outer/inner split Fermi contours but also has inversion symmetry: a $NbSe_2$ bilayer. In that case every state is spin-degenerate, and anomalous averages will appear in the pure singlet channel,

$$\begin{aligned} d'_{o,\mathbf{k}} &= d'_{o,-k} = \overline{|K,o,\uparrow\rangle|K',o,\downarrow\rangle} - \overline{|K,o,\downarrow\rangle|K',o,\uparrow\rangle} \\ d_{i,\mathbf{k}} &= d_{i,-\mathbf{k}} = -\overline{|K,i,\downarrow\rangle|K',i,\uparrow\rangle} + \overline{|K,i,\uparrow\rangle|K',i,\downarrow\rangle} \end{aligned} \tag{11}$$

Note that in an Ising superconductor Eq. (10) there is no such thing as $d_{-\mathbf{k}}$, because a K, o state has *only* the ↑, and a K, i state has *only* the ↓ one, making this conceptually different from a non-Ising bilayer with the same geometry of the Fermi surface.

We illustrate this in Fig. 3: in panels a and b, we show possible superconducting states in the more familiar non-Ising, inversion-symmetric, bilayer superconductor: both inner and outer K, K' Fermi circles carry an order parameter (colored by its sign) for each **k** and −**k**. On the contrary, in panels c and d, we show a schematic of possible superconducting states in an Ising superconductor with the same Fermi surface. In this case, we only draw *one* contour around each K or K' point to emphasize that we have defined an order parameter Eq. (10) for a k point, we cannot define one for −**k**. Note that if the EPC in a bilayer or a monolayer was dominated by the $K_o - K'_i$ scattering (which is not the case, per our calculations), then the s state (a, c) would be close in energy to the f state (b, d), despite the interaction being purely EPC (Table 2).

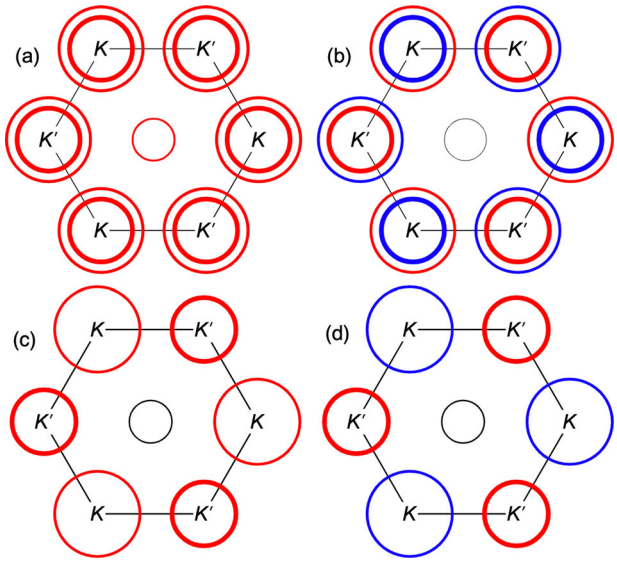

Fig. 3 Schematic illustration of the Ising superconductor pairing symmetry. Schematic illustration of possible pairing symmetry in a regular superconductor with hybridization-split, Kramers-degenerate Fermi surfaces (with inversion symmetry), and in an Ising superconductor. Splitting and superconductivity on the Γ pocket are neglected. The color shows the sign of the order parameter. **a**, **c** correspond to an s-wave, and **b**, **d** to a f-wave symmetry. Note that in the IS the order parameter cannot be independently defined for **k** and −**k**, so only one is shown.

In our case of an Ising superconductor, the dominance of the EPC $K_o - K'_i$ scattering fixes the phases as shown in Fig. 3c. This essentially excludes the possibility of a predominantly triplet state, albeit generates a small (≈ 10%) triplet admixture.

Let us now turn to spin fluctuations (Table 2). Quantitatively, as conjectured in ref. [17], the SF coupling in the $K - K'$ channels is small, and so is the intraband coupling. There is a sizeable $K_o - K_i$ coupling, which does favor triplet, but it is not strong enough, and, surprisingly, an even stronger contribution appears in the $K - \Gamma$ channels. As a result, not only a triplet f state, corresponding to Fig. 3d, is unstable compared to the s state, it is not even competitive, but an $s_\pm$ state, where the order parameter in the Γ pocket is flipped compared to the K pockets.

At the level of accuracy available in our calculations, we can exclude the s–f Leggett mode, recently proposed for tunneling measurements[20], but cannot exclude the possibility of a Leggett mode associated with the phase fluctuations between the Γ and K pockets. This we will address in more detail later. We can also exclude the recently proposed nematic superconductivity ascribed to a close competition between s-wave and a higher-angular-momenta state[54].

It is still instructive to compare our results with the simple linearized BCS solution that requires the order parameters near the transition temperature to be proportional to the eigenvectors of the matrix λ, corresponding to its largest eigenvalue. Diagonalizing the matrix in Table 3, we get the largest eigenvalue $\lambda_{max} = 1.24$, and the corresponding order parameters as shown in the penultimate line in the same table.

There is rather little difference between the inner and the outer pockets, again in agreement with the full Eliashberg solution, about 10%. The Γ pocket order parameter is less than half of those on the K pockets. Earlier we have discussed the potential ramifications of this for tunneling.

Table 2. Same as in Table 3, but for spin fluctuations induced coupling.

	Γ	K_i, K_i'	K_o, K_o'
$N(E_F)$	0.839	0.632	0.734
Γ	−0.647	−0.420	−0.495
K_i, K_i'	−0.420	−0.214	−0.446
K_o, K_o'	−0.495	−0.446	−0.218

Note that the dynamic logarithmic renormalization is not taken into account yet.

Table 3. Calculated electron–phonon coupling matrix V_{ij} in eV.

	Γ	K_i, K_i'	K_o, K_o'
$N(E_F)$	0.839	0.632	0.734
Γ	0.150	0.390	0.322
K_i, K_i'	0.390	0.222	1.432
K_o, K_o'	0.321	1.432	0.169
1.24	0.293	0.706	0.645
0.00	0.935	−0.243	−0.258

The subscripts "*o*" and "*i*" stand for the outer and inner pocket around the corresponding point. We do not distinguish the outer and inner pockets around Γ. The first line gives the partial DOS, N_i, on each Fermi surface pocket in states eV^{-1} f.u.$^{-1}$. The last two lines give the two largest eigenvalues of the $\lambda_{ij} = V_{ij}N_j$ matrix, and the eigenvectors giving the relative order parameters.

Recent tunneling data have suggested the appearance of a superconducting collective mode interpreted as a Leggett mode between the s-wave state and a proximate f-wave triplet channel[20]. In this section, we use our first principles results to examine the possibility that this mode is due to fluctuations of the order parameter phase between the *K* pockets and the Γ pockets.

In this section, we have delineated an analytical evaluation of a self-consistent solution of the Bardeen–Cooper–Schrieffer theory of superconductivity, based on parameters derived from first-principles calculations. In order to solve for the Leggett modes, we adopt the following scheme as described below.

1. First, we assume that the superconducting order parameter Δ varies very little within each individual sheet of the $NbSe_2$ Fermi surface (FS), while differing significantly between the different FS sheets. Such assumptions lead to the following expression for the superconducting order parameter:
$$\Delta_i = \sum_i \Lambda_{ij}\Delta_j F(\Delta_j, T) \tag{12}$$
where
$$F = \int_0^{\omega_D} dE \tanh\left(\left(\sqrt{E^2+\Delta^2}\right)/2T\right)/\sqrt{E^2+\Delta^2} \tag{13}$$
Note that here the matrix Λ_{ij} characterizes the electron–phonon interaction and can be expressed in terms of the convolution of the pairing interaction due to electron–phonon coupling and the band-resolved density of states as $\Lambda_{ij} = V_{ij}N_j$, whereas the temperature dependence of the superconducting gap function is dictated by the functional form *F*.
2. Second, in order to incorporate the effect of spin-fluctuation contributions to the superconducting pairing interaction in the monolayer, a fluctuation parameter *α* has been defined to establish the effect of spin-fluctuations on the same footing as that of electron–phonon coupling. The material-specific fluctuation term *α*, that accounts for the effect of renormalized spin fluctuation is of negative sign. We define the renormalized matrix $\Lambda_{ij} = \Lambda_{ij}^{ep} + \alpha\Lambda_{ij}^{sf}$, which denotes the total (electron–phonon coupling and spin fluctuation) pairing interaction term for solving the BCS equations.
3. Third, we choose starting values of the gap parameters Δ_1 and Δ_2, respectively, where Δ_1 and Δ_2 refer to the superconducting order parameters for the Γ and *K* points of the FS sheets and solve the above BCS equations self-consistently in order to obtain an analytical solution of the superconducting gap equation as a function of temperature.
4. Fourth, we determine the value of the material-specific spin-fluctuation parameter *α*, and hence the renormalized matrix Λ_{ij}, heuristically by incorporating the values of Δ_1 and Δ_2 obtained from our first-principles calculations of electron–phonon coupling and spin fluctuations obtained from the solution of the Eliashberg equations from first-principles using the EPW software.
5. Finally, we utilize the parameters obtained from first principles and the analytical solution of the self-consistent BCS equations, in order to provide a quantitative estimate of the frequency of the superconducting Leggett mode for comparison with experimental observations. This is achieved by solving the following equation
$$\omega_L^2 = \frac{4\Delta_1\Delta_2 V_{12}}{detV}\,\frac{N_1 f_1 + N_2 f_2}{N_1 N_2 f_1 f_2}, \tag{14}$$
where $f(\omega) = \sin^{-1}\omega/\omega\sqrt{1-\omega^2}$. Here, Δ_1 and Δ_2 again refer to the superconducting order parameters for the Γ and *K* points respectively of the Fermi surface. Thus, self-consistent solution of the above set of equations lead to the quantitative estimate of the Leggett frequency.

In order to further reconstruct the gap structure from first-principles calculations, we proceed with the pairing interaction matrix derived from the solution of the Eliashberg equations, and implement the required modifications to analytically solve the BCS equations. Figure 4a, b illustrates the analytical solution of the pairing interaction, by fitting the two-gap BCS equations with that of our first-principles calculations without and with the inclusion of spin fluctation effects, respectively, in addition to electron–phonon coupling. The ensuing elements of the interaction matrix utilized for our analytical solution of the self-consistent BCS equations are $V_{11} = 0.2957$, $V_{12} = V_{21} = 0.0558$, and $V_{22} = 0.5997$ eV, respectively. The density of states estimated from first-principles N_1 and N_2 are 0.8392 and 1.365 states/(eV f.u.), which correspond to that of the Γ and *K* segments of the Fermi surface. Finally, the magnitudes of the superconducting gaps resulting from solving the Eliashberg equations Δ_1 and Δ_2 are 0.15 and 0.55 meV for the Γ and *K* segments of the Fermi segments. We note that, the frequency of the Leggett mode obtained from resonant phase fluctuations, should, in principle, be larger than the magnitude of the minimum superconducting gap of 0.15 meV from that of the Γ point. Interestingly, our calculation of the frequency of the Leggett mode, yields a value of 0.29 meV for the Leggett mode frequency.

In the tunneling experiments, that recently reported the observation of soft collective modes in monolayer $NbSe_2$[20], new satellite peaks are seen at integer multiples of the fundamental frequency in the single layer samples. These satellites are thought to have their origin in collective Leggett modes in the experimentally grown monolayers. Experimental conductance spectrum revealed an average BCS gap of $\Delta_{BCS} = 0.4$ meV, a resonant Leggett mode frequency $\Omega_L = 0.53$ meV and the ratio $\Omega_L/2\Delta_{BCS} = 0.66$. Our self-consistent analytical solution and first-principles calculations including electron–phonon coupling and spin-fluctuation contribution correspond to an estimated average

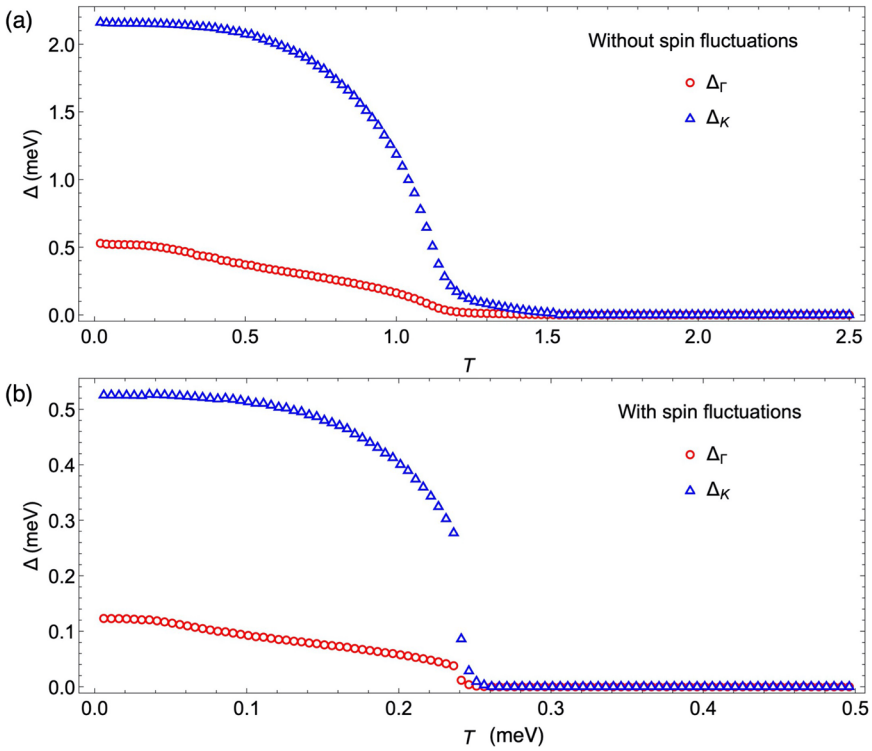

Fig. 4 Analytical solution of the two-gap BCS equations. Analytical evaluation of the pairing interaction, by fitting the two-gap BCS equations to that of our first-principles calculations including (**a**) electron–phonon interaction and **b** both electron–phonon interaction and spin-fluctuation effects evaluated utilizing density functional theory artificially stabilized by Hubbard interactions combined with spin-spiral methodology.

$\Delta_{BCS} = 0.35$ meV, the frequency of the collective Leggett mode $\omega_L = 0.29$ meV and the ratio $\omega_L/2\Delta_{BCS} = 0.41$. A final note worth mentioning in passing is that while an amplitude Higgs mode[55,56] has also been observed in the superconducting bulk $NbSe_2$[57,58] due to the mixing with collective CDWs, such a mode can be discarded in monolayer $NbSe_2$, since the CDW mode energy is considerably larger than the superconducting order parameter in the monolayer case.

Utilizing state-of-the-art DFT and Wannier interpolation formalism, we have calculated the momentum-resolved electron–phonon coupling interaction in the single layer $NbSe_2$. The two main findings are: (1) the overall strength of this interaction is such that the superconducting critical temperature and the gap parameter are substantially overestimated, and (2) the leading contribution to the electron–phonon coupling comes from the intepocket scattering between the K and K' pockets of the Fermi surface. We suggest that the phonon-induced superconductivity in single $NbSe_2$, and likely in other similar materials, bulk or monolayer, is weakened by spin fluctuations.

We find that, if the standard static formulation of the Berk-Schrieffer-Scalapino formalism is adopted, realistic estimates of the strength of electron-spin-fluctuation coupling lead to complete suppression of superconductivity, in dramatic contradiction with the experiment. We argue that this is due to neglect of the retardation effects, weakening the effect of spin-fluctuations logarithmically, analogous to, but not as strong as the famous Tolmachev–Morel–Anderson renormalization of the Coulomb repulsion.

If the latter is accounted for, the structure of the superconducting order parameter changes notably from a pure phonon mechanism, albeit the fact that the strongest interaction occurs in the $K - K'$ channel, remains, and even becomes stronger, and the overall agreement with the experiment is satisfactory. We find that the leading instability is in the s_{++} wave channel, and the subleading one in the $s_{\pm}$ channel, where the sign of the (smaller) order parameter on the Γ centered pocket is flipped with respect to the K, K' pockets.

We estimate the frequency of the Leggett mode driven by this subleading instability, and find it to be in reasonable agreement with the recently claimed Leggett mode observation in the STM spectroscopy.

METHODS

First-principles calculations were performed with density functional theory (DFT) using the Quantum ESPRESSO (QE)[59] code. We employed optimized norm-conserving Vanderbilt (ONCV) pseudopotentials[60,61] with the Perdew–Burke–Ernzerhof (PBE) exchange-correlation functional in the generalized gradient approximation[62], where the Nb $4s^2 4p^6 4d^3 5s^2$ and Se $4s^2 4p^4$ orbitals were included as valence electrons. All calculations were performed for the experimental lattice parameters at ambient pressure[63] with relaxed internal coordinates. We used a plane wave kinetic-energy cutoff value of 80 Ry, and the electronic and vibrational Brillouin zones (BZ) were sampled using $24 \times 24 \times 1$ and $12 \times 12 \times 1$ points, respectively. A Methfessel and Paxton smearing[64] width of 0.025 Ry was used in order to resolve the CDW instability. The superconductivity calculations were performed with a modified version of the EPW code[41,65,66]. We used 22 maximally localized Wannier functions[67,68] (five d-orbitals for each Nb atom and three p-orbitals for each Se atom) and a uniform Γ-centered $12 \times 12 \times 1$ electron-momentum grid. Eqs. (6) and (7) were evaluated on a uniform $240 \times 240 \times 1$ **k**-point grid and a uniform $120 \times 120 \times 1$ **q**-point grid. The Dirac deltas were replaced by Gaussians of width 2.5 meV (electrons) and 0.1 meV (phonons), and the Matsubara frequency cutoff was set to 1 eV. The momentum-dependent static spin susceptibility $\chi_{\mathbf{q}}(0)$ in the random-phase approximation (RPA) and the Stoner parameter I

were obtained in our previous work[19]. The DFT Stoner factor was found to be $I = 0.646$ eV f.u.$^{-1}$ and the spin susceptibility was divided by 6.466×10^{-5} to convert from emu mol^{-1} to eV^{-1} units used in the current study. The analytical solution of the two-gap BCS equations were performed utilizing the Mathematica Wolfram Language software package[69].

DATA AVAILABILITY

The data that support the findings of this study are available from the corresponding authors upon reasonable request.

CODE AVAILABILITY

The Quantum ESPRESSO, Wannier90, and EPW programs used in this work are publicly available. A modified version of EPW for superconductivity calculations with spin fluctuations is available upon request.

Received: 3 October 2022; Accepted: 3 April 2023;
Published online: 26 April 2023

REFERENCES

1. Xing, Y. et al. Ising superconductivity and quantum phase transition in macro-size monolayer $NbSe_2$. *Nano Lett.* **17**, 6802–6807 (2017).
2. Wang, C. et al. Type-II Ising superconductivity in two-dimensional materials with spin-orbit coupling. *Phys. Rev. Lett.* **123**, 126402 (2019).
3. Xi, X. et al. Ising pairing in superconducting $NbSe_2$ atomic layers. *Nat. Phys.* **12**, 139 (2016).
4. Dvir, T. et al. Spectroscopy of bulk and few-layer superconducting $NbSe_2$ with van der Waals tunnel junctions. *Nat. Commun.* **9**, 598 (2018).
5. Möckli, D. & Khodas, M. Robust parity-mixed superconductivity in disordered monolayer transition metal dichalcogenides. *Phys. Rev. B* **98**, 144518 (2018).
6. Fischer, M. H., Sigrist, M., Agterberg, D. F. & Yanase, Y. Superconductivity and local inversion-symmetry breaking. *Annu. Rev. Condens. Matter Phys.* **14**, 153–172 (2023).
7. Wickramaratne, D., Haim, M., Khodas, M. & Mazin, I. I. Magnetism-driven unconventional effects in Ising superconductors: role of proximity, tunneling, and nematicity. *Phys. Rev. B* **104**, L060501 (2021).
8. de la Barrera, S. C. et al. Tuning Ising superconductivity with layer and spin-orbit coupling in two-dimensional transition-metal dichalcogenides. *Nat. Commun.* **9**, 1427 (2018).
9. Lu, J. M. et al. Evidence for two-dimensional Ising superconductivity in gated MoS_2. *Science* **350**, 1353–1357 (2015).
10. Sergio, C. B. et al. Tuning Ising superconductivity with layer and spin-orbit coupling in two-dimensional transition-metal dichalcogenides. *Nat. Commun.* **9**, 1427 (2018).
11. Zhu, Z. et al. Discovery of segmented Fermi surface induced by Cooper pair momentum. *Science* **374**, 1381–1385 (2021).
12. Yi, H. et al. Crossover from Ising- to Rashba-type superconductivity in epitaxial Bi2Se3/monolayer $NbSe_2$heterostructures. *Nat. Mat.* **21**, 1366–1372 (2022).
13. Hamill, A. et al. Two-fold symmetric superconductivity in few-layer $NbSe_2$. *Nat. Phys.* **17**, 949–954 (2021).
14. Huang, B. et al. Electrical control of 2D magnetism in bilayer CrI_3. *Nat. Nanotechnol.* **13**, 544–548 (2018).
15. Jiang, S., Li, L., Wang, Z., Mak, F. K. & Shan, J. Controlling magnetism in 2D CrI_3 by electrostatic doping. *Nat. Nanotechnol.* **13**, 549–553 (2018).
16. Tian, S. et al. Ferromagnetic van der Waals crystal VI_3. *J. Am. Chem. Soc.* **141**, 5326–5333 (2019).
17. Wickramaratne, D., Khmelevskyi, S., Agterberg, D. F. & Mazin, I. I. Ising superconductivity and magnetism in $NbSe_2$. *Phys. Rev. X* **10**, 041003 (2020).
18. Divilov, S. et al. Magnetic correlations in single-layer $NbSe_2$. *Comput. Mater. Sci.* **33**, 295804 (2021).
19. Das, S. & Mazin, I. I. Quantitative assessment of the role of spin fluctuations in 2D Ising superconductor $NbSe_2$. *Comput. Mater. Sci.* **200**, 110758 (2021).
20. Wan, W. et al. Observation of superconducting collective modes from competing pairing instabilities in single-layer $NbSe_2$. *Adv. Mater.* **34**, 2206078 (2022).
21. Mazin, I. I. & Cohen, R. E. Notes on the static dielectric response function in the density functional theory. *Ferroelectrics* **194**, 263–270 (1997).
22. Leroux, M. et al. Strong anharmonicity induces quantum melting of charge density wave in $2H-NbSe_2$ under pressure. *Phys. Rev. B* **92**, 140303 (2015).
23. Guster, B. et al. Coexistence of elastic modulations in the charge density wave state of $2H-NbSe_2$. *Nano Lett.* **19**, 3027–3032 (2019).
24. Calandra, M., Mazin, I. I. & Mauri, F. Effect of dimensionality on the charge-density wave in few-layer $2H$-$NbSe_2$. *Phys. Rev. B* **80**, 241108 (2009).
25. Kvashnin, Y. et al. Coexistence of superconductivity and charge density waves in tantalum disulfide: experiment and theory. *Phys. Rev. Lett.* **125**, 186401 (2020).
26. Heil, C. et al. Origin of superconductivity and latent charge density wave in NbS_2. *Phys. Rev. Lett.* **119**, 087003 (2017).
27. Xi, X. et al. Enhanced electron-phonon interactions in mono- and few-layer $NbSe_2$ result in a significantly increased transition temperature of charge density waves compared with values in the bulk. *Nat. Nanotechnol.* **10**, 765–769 (2015).
28. Yokoya, T. et al. Fermi surface sheet-dependent superconductivity in $2H-NbSe_2$. *Science* **294**, 2518–2520 (2001).
29. Sanna, A. et al. Real-space anisotropy of the superconducting gap in the charge-density wave material 2H-$NbSe_2$. *NPJ Quantum Mater.* **7**, 174425 (2011).
30. Wan, W. et al. Nontrivial doping evolution of electronic properties in Ising-superconducting alloys. *Adv. Mater.* **34**, 2200492 (2022).
31. Khestanova, E. et al. Unusual suppression of the superconducting energy gap and critical temperature in atomically thin $NbSe_2$. *Nano Lett.* **18**, 2623–2629 (2018).
32. Lian, C.-S., Si, C. & Duan, W. Unveiling charge-density wave, superconductivity, and their competitive nature in two-dimensional $NbSe_2$. *Nano Lett.* **18**, 2924–2929 (2018).
33. Zheng, F. & Feng, J. Electron-phonon coupling and the coexistence of superconductivity and charge-density wave in monolayer $NbSe_2$. *Phys. Rev. B* **99**, 161119 (2019).
34. Lian, C.-S. et al. Intrinsic and doping-enhanced superconductivity in monolayer $1H-TaS_2$: critical role of charge ordering and spin-orbit coupling. *Phys. Rev. B* **105**, L180505 (2022).
35. Foner, S. & McNiff, E. Upper critical fields of layered superconducting $NbSe_2$ at low temperature. *Phys. Lett. A* **45**, 429–430 (1973).
36. Iavarone, M. et al. Effect of magnetic impurities on the vortex lattice properties in $nbse_2$ single crystals. *Phys. Rev. B* **78**, 174518 (2008).
37. Cho, K. et al. Using controlled disorder to probe the interplay between charge order and superconductivity in $NbSe_2$. *Nat. Commun.* **9**, 2798 (2018).
38. Moulding, O., Osmond, I., Flicker, F., Muramatsu, T. & Friedemann, S. Absence of superconducting dome at the charge-density-wave quantum phase transition in $2H-NbSe_2$. *Phys. Rev. Res.* **2**, 043392 (2020).
39. Suderow, H., Tissen, V. G., Brison, J. P., Martínez, J. L. & Vieira, S. Pressure Induced effects on the fermi surface of superconducting 2H-$NbSe_2$. *Phys. Rev. Lett.* **95**, 117006 (2005).
40. Giustino, F. Electron-phonon interactions from first principles. *Rev. Mod. Phys.* **89**, 015003 (2017).
41. Poncé, S., Margine, E., Verdi, C. & Giustino, F. EPW: electron-phonon coupling, transport and superconducting properties using maximally localized Wannier functions. *Comp. Phys. Commun.* **209**, 116–133 (2016).
42. Berk, N. F. & Schrieffer, J. R. Effect of ferromagnetic spin correlations on superconductivity. *Phys. Rev. Lett.* **17**, 433–435 (1966).
43. Scalapino, D. Superconductivity and spin fluctuations. *J. Low Temp. Phys.* **117**, 179–188 (1999).
44. Fay, D. & Appel, J. Coexistence of *p*-state superconductivity and itinerant ferromagnetism. *Phys. Rev. B* **22**, 3173–3182 (1980).
45. Scalapino, D. J. A common thread: the pairing interaction for unconventional superconductors. *Rev. Mod. Phys.* **84**, 1383–1417 (2012).
46. Bekaert, J., Aperis, A., Partoens, B., Oppeneer, P. M. & Milošević, M. V. Advanced first-principles theory of superconductivity including both lattice vibrations and spin fluctuations: the case of FeB_4. *Phys. Rev. B* **97**, 014503 (2018).
47. Tolmachev, V. V. Logarithmic criterion for superconductivity. *Dokl. Akad. Nauk SSSR* **140**, 563–566 (1961).
48. Morel, P. & Anderson, P. W. Calculation of the superconducting state parameters with retarded electron-phonon interaction. *Phys. Rev.* **125**, 1263–1271 (1962).
49. Kampf, A. & Schrieffer, J. R. Pseudogaps and the spin-bag approach to high-T_c superconductivity. *Phys. Rev. B* **41**, 6399–6408 (1990).
50. Kostur, V. N. & Mitrović, Bcv Superconducting T_c for a model spin-fluctuation spectrum with four sharp peaks in the corners of the Brillouin zone. *Phys. Rev. B* **51**, 6064–6075 (1995).
51. *Eliashberg Theory - Giovanni A.C. Ummarino*, Vol. 3 of *Lecture Notes of the Autumn School Correlated Electrons 2013 Eva Pavarini, Erik Koch, and Ulrich Schollwöck* (Forschungszentrum Jülich GmbH Institute for Advanced Simulation. https://www.cond-mat.de/events/correl13/ (2013).
52. Bianco, R., Monacelli, L., Calandra, M., Mauri, F. & Errea, I. Weak dimensionality dependence and dominant role of ionic fluctuations in the charge-density-wave transition of $NbSe_2$. *Phys. Rev. Lett.* **125**, 106101 (2020).
53. Parker, D., Vavilov, M. G., Chubukov, A. V. & Mazin, I. I. Coexistence of superconductivity and a spin-density wave in pnictide superconductors: gap symmetry and nodal lines. *Phys. Rev. B* **80**, 100508 (2009).

54. Cho, C.-W. Nodal and Nematic Superconducting Phases in $NbSe_2$ Monolayers from Competing Superconducting Channels. *Phys. Rev. Lett.* **129**, 087002 (2022).
55. Pekker, D. & Varma, C. Amplitude/Higgs modes in condensed matter physics. *Annu. Rev. Condens. Matter Phys.* **6**, 269–297 (2015).
56. Shimano, R. & Tsuji, N. Higgs mode in superconductors. *Annu. Rev. Condens. Matter Phys.* **11**, 103–124 (2020).
57. Méasson, M.-A. et al. Amplitude Higgs mode in the 2H − $NbSe_2$ superconductor. *Phys. Rev. B* **89**, 060503 (2014).
58. Grasset, R. et al. Higgs-mode radiance and charge-density-wave order in 2H − $NbSe_2$. *Phys. Rev. B* **97**, 094502 (2018).
59. Giannozzi, P. et al. Advanced capabilities for materials modelling with QUANTUM ESPRESSO. *J. Phys. Condens. Matter* **29**, 465901 (2017).
60. Hamann, D. R. Optimized norm-conserving Vanderbilt pseudopotentials. *Phys. Rev. B* **88**, 085117 (2013).
61. Schlipf, M. & Gygi, F. Optimization algorithm for the generation of ONCV pseudopotentials. *Comput. Phys. Commun.* **196**, 36–44 (2015).
62. Perdew, J. P., Burke, K. & Ernzerhof, M. Generalized gradient approximation made simple. *Phys. Rev. Lett.* **77**, 3865–3868 (1996).
63. Weber, F. et al. Extended phonon collapse and the origin of the charge-density wave in 2*H* − $NbSe_2$. *Phys. Rev. Lett.* **107**, 107403 (2011).
64. Methfessel, M. & Paxton, A. T. High-precision sampling for Brillouin-zone integration in metals. *Phys. Rev. B* **40**, 3616–3621 (1989).
65. Giustino, F., Cohen, M. L. & Louie, S. G. Electron-phonon interaction using Wannier functions. *Phys. Rev. B* **76**, 165108 (2007).
66. Margine, E. R. & Giustino, F. Anisotropic Migdal-Eliashberg theory using Wannier functions. *Phys. Rev. B* **87**, 024505 (2013).
67. Marzari, N., Mostofi, A. A., Yates, J. R., Souza, I. & Vanderbilt, D. Maximally localized Wannier functions: theory and applications. *Rev. Mod. Phys.* **84**, 1419–1475 (2012).
68. Pizzi, G. et al. Wannier90 as a community code: new features and applications. *J. Phys. Condens. Matter* **32**, 165902 (2020).
69. Wolfram Research Inc. Mathematica, Version 13.1. https://www.wolfram.com/mathematica. (Champaign, IL, 2022).
70. Towns, J. et al. XSEDE: accelerating scientific discovery. *Comput. Sci. Eng.* **16**, 62–74 (2014).

ACKNOWLEDGEMENTS

The work at GMU (S.D. and I.I.M.) was supported by Office of Naval Research through grant N00014-20-1-2345. H.P. and E.R.M. acknowledge support from the National Science Foundation (NSF) under Grant No. DMR-2035518 and Grant No. OAC-2103991 for method development, superconductivity analysis, and code development. D.F.A. was supported by the U.S. Department of Energy, Office of Basic Energy Sciences, Division of Materials Sciences and Engineering, under Award No. DE-SC0021971. This work used the Extreme Science and Engineering Discovery Environment (XSEDE)[70] which is supported by NSF Award No. ACI-1548562. Specifically, this work used Comet at the San Diego Supercomputer Center through allocation TG-DMR180071.

AUTHOR CONTRIBUTIONS

E.R.M, I.I.M., and D.F.A. designed the project. E.R.M., H.P., and S.D. performed the first-principles electronic band structure, electron–phonon calculations and computational analysis. S.D., E.R.M., and I.I.M. performed the momentum-dependent spin susceptibility calculations, and estimation of spin-fluctuation interaction. S.D. carried out the analytical evaluation of the pairing interaction, fitting of the two-gap BCS equations, and quantitative estimation of the Leggett mode. I.I.M. and D.F.A. provided theoretical and analytical insights, respectively. All authors contributed to the analysis and discussion of the results. S.D., E.R.M., and I.I.M. wrote the manuscript with input from all co-authors.

COMPETING INTERESTS

The authors declare no competing interests.

ADDITIONAL INFORMATION

Correspondence and requests for materials should be addressed to S. Das.

Reprints and permission information is available at http://www.nature.com/reprints

Publisher's note Springer Nature remains neutral with regard to jurisdictional claims in published maps and institutional affiliations.